J. Fluid Mech. (1986), *vol.* 170, *pp.* 527–544
Printed in Great Britain

Vortex shedding and lock-on of a circular cylinder in oscillatory flow

By C. BARBI, D. P. FAVIER, C. A. MARESCA
Institut de Mécanique des Fluides, UM34-C.N.R.S., Marseille, France

AND D. P. TELIONIS
Virginia Polytechnic Institute and State University, Blacksburg, Virginia, USA

(Received 1 November 1984 and in revised form 20 March 1986)

An experimental study has been made of a circular cylinder in steady and oscillatory flow with non-zero mean velocity up to a Reynolds number of 40000. The results for the stationary cylinder are in close agreement with previously published data. Skin-friction measurements revealed the amplitude of fluctuation of the boundary layer for different angular locations. It has been universally accepted that bluff bodies shed vortices at their natural frequency of shedding (Strouhal frequency), or, when synchronized with an external unsteadiness, at the frequency of the disturbance or half of it, depending of the direction of the unsteadiness. Our findings, instead, indicate that the shedding frequency may vary smoothly with the driving frequency before locking on its subharmonic. Moreover, the present results indicate that, at the lowest frequency limit of lock-on, vortices are shed simultaneously on both sides of the model. A more traditional alternate pattern of vortex shedding is then recovered at higher driving frequencies.

1. Introduction

The understanding of the characteristics of vibrations induced by vortex shedding is of great importance in the design of structures such as heat exchangers, offshore platforms, power cables, etc. During the past twenty years, several cases of malfunctioning or damage due to aeroelastic instabilities have been reported (Sainsbury & King 1971). Studies related to industrial failures and the solutions proposed for design improvement (Chen 1968) confirm the aerodynamic origin of the problem and are linked to fundamental work in fluid dynamics.

The flow around cylinders has always been a challenge to investigators. In the presence of external disturbances the flow field is even more complex. The experimental work done on cylinders in wind tunnels has revealed the important role played by 'locking-on' of the shedding frequency on the disturbance. 'Locking-on' was first studied on self-induced oscillations of lightly damped cylinders (Ferguson & Parkinson 1967). In order to better understand the parameters which influence the lock-on phenomenon, investigators in the last decade have forced a cylinder to oscillate in uniform flow. Tanida, Okajima & Watanabe (1973) showed evidence of locking-on due to cross-stream and in-line vibrations of a cylinder. The boundary zones of lock-on are related to the reduced amplitude, A/D (where D is the cylinder diameter) as reported by Stansby (1976) for transverse oscillations and Griffin & Ramberg (1976) for in-line oscillations.

These studies and the analysis which followed (Ericsson 1980) have emphasized

the role played by the oscillations of a cylinder in uniform flow. The aim of this paper is to continue this line of fundamental work in an attempt to cast some light on a still-debated question: does lock-on occur in the case of a fixed cylinder subject to an oscillatory incident stream with non zero mean velocity? Earlier works (Hatfield & Morkovin 1973) were inconclusive, probably because both the parameter A/D and the fluid oscillation frequency range were too low. Ericsson (1980) states: 'Whether or not lock-in will also occur if the relative velocity change is obtained through harmonic perturbation of the free stream velocity $U(t) = U_\infty[1 + (\Delta U/U_\infty \sin 2\pi Ft)]$ is not clear'. The answer to this question is of fundamental interest and could provide practical solutions for heat-exchanger design (Sagner 1981).

This study has been conducted in two facilities: a water tunnel at Virginia Polytechnic Institute and State University (VPI & SU), USA, and a wind tunnel at Institut de Mécanique des Fluides de Marseille (IMFM), France, with two different experimental set-ups. The flows around circular cylinders have been investigated for Reynolds numbers $R_D = V_\infty D/\nu$ of 3000–40000 (here V_∞ is the free-stream velocity and ν is the kinematic viscosity).

The flow oscillation in water ranged from 0.2 to 2.0 Hz with reduced amplitudes $\lambda = \Delta V/\overline{V} = 0.1$ to 0.25, and in air from 1.2 to 6.75 Hz with $\lambda = 0.1$ to 0.5. The complex flow field around the cylinder was studied using different measuring techniques suited to unsteady flows. The skin friction was measured to relate the boundary-layer behaviour to the external flow field obtained from pressure measurements. Laser-Doppler velocimetry and hot-wire anemometry were employed in water and in air respectively. The energy spectrum deduced from velocity measurements was correlated with lift and drag on the cylinder. Finally, flow visualization was used to supplement the quantitative results.

Lock-on studies have previously been conducted by the present group as reported in a sequence of non-archival publications (Jones 1980; Jones, Telionis & Barbi 1981; Jones, Barbi & Telionis 1981; Barbi, Favier & Maresca 1981) and the material of this paper overlaps with them.

2. Experimental arrangements

The two series of experiments at VPI & SU and IMFM were similar, both involving velocity measurements and flow visualizations. However, at IMFM, it was also possible to take measurements of unsteady skin friction, pressure and forces.

2.1. *Facilities*

The water tunnel at VPI & SU is a closed-circuit facility with a contraction ratio of 6:1 leading to a 25×30 cm^2 test section. The velocity ranges from 0.01 m/s to 3 m/s with a turbulence level from 0.4 to 0.8%. The flow oscillations were induced by means of flaps downstream of the test section (Jones *et al.* 1981*b*).

The IMFM facility is a low-turbulence, open-circuit wind tunnel with a 3 m long rectangular test section (0.5×1.0 m^2). The turbulence level is reduced to 0.2% by screens located upstream of the nozzle, over a velocity range of 2.5 m/s–20 m/s in steady conditions, and to 0.8% in pulsating flow. In order to obtain a sinusoidal variation of the velocity in the test section, part of the flow is bypassed by two motor-driven flaps before reaching the settling chamber (Maresca, Favier & Rebont 1978). Figures 1 (*a*, *b*) display the velocity profiles obtained in both facilities. In air, the velocity signal is averaged over 20 cycles and the Fourier-series analysis indicates that for all frequencies the second harmonic is around 20% of the fundamental and

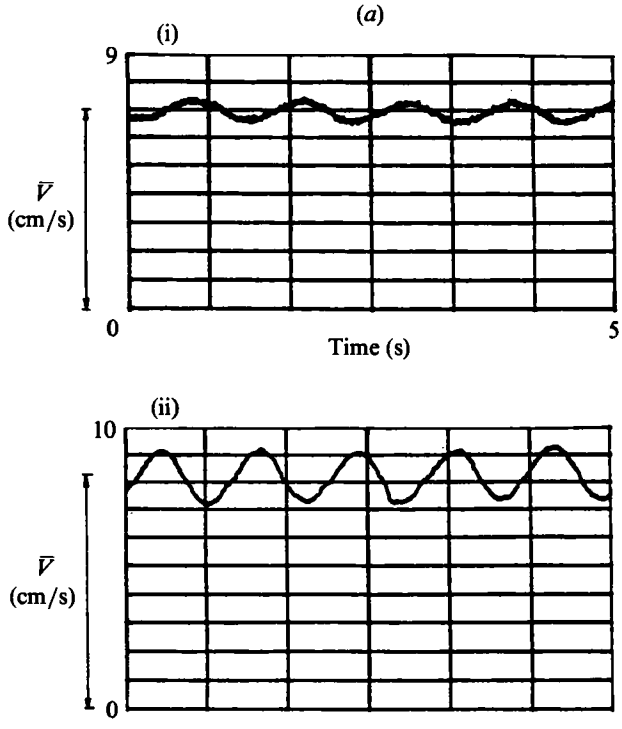

FIGURE 1(*a*). For caption see next page.

the third is less than 9 %. It has been checked by means of two pressure transducers on the wind-tunnel wall that there is no phase lag between the two corresponding signals, thus confirming the absence of standing acoustic waves.

2.2. *Models and measurement techniques*

In the water tunnel, the velocity measurements were carried out using a one-channel DISA 55 laser-Doppler velocimeter and a FFT analyser, described by Koromilas & Telionis (1980). The system was arranged in a forward-scatter mode and the photodetector signal was fed to a tracker. The optical bench was mounted on a lathe bed, allowing manual traversing of the measuring volume. Measurements were obtained in the wake of the cylinder but we found that clear vortex-shedding characteristics are displayed at points about one-half cylinder radius above and downstream of the point of separation. Although three fixed fibreglass cylinders were tested of diameter 1, 2 and 3.5 cm, only the results obtained with the largest one are presented in this paper. This cylinder was fitted with dye ports as shown in figure 2. The reader will find more results in Jones (1980).

In the wind tunnel, the velocity was measured using a DISA 55P05 hot-wire probe, a DISA 55 M series anemometer and a DISA 55D10 linearizer (figure 3). The anemometer was also used to process the hot-film friction gauge (fabricated at IMFM) which was mounted flush on the surface of the cylinder. The probe was made of a plastic base and a nickel film of 0.1 mm width and a few microns thickness (figure 4*a*). This gauge has been used to obtain qualitative information on the boundary-layer behaviour, the location of stagnation and separation. Time response of this type of probe is usually around 10 ms. An Endevco 8507-2 series pressure gauge was

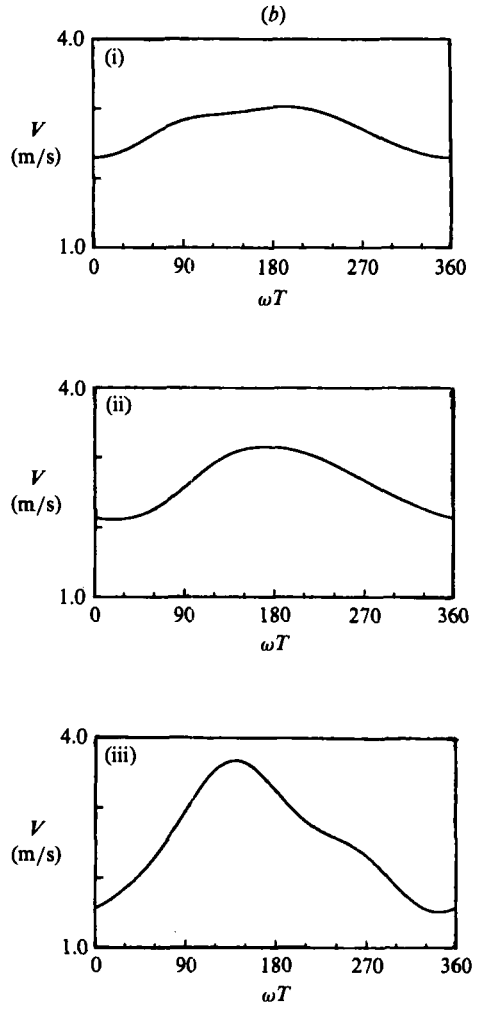

FIGURE 1. (*a*) Velocity waveforms in water. (i) $F = 0.2$ Hz, $\lambda = 0.065$; (ii) $\lambda = 0.125$. (*b*) Velocity waveforms in air. (i) $F = 1.5$ Hz, $\lambda = 0.13$; (ii) $F = 2.6$ Hz, $\lambda = 0.220$; (iii) $F = 4.5$ Hz, $\lambda = 0.39$.

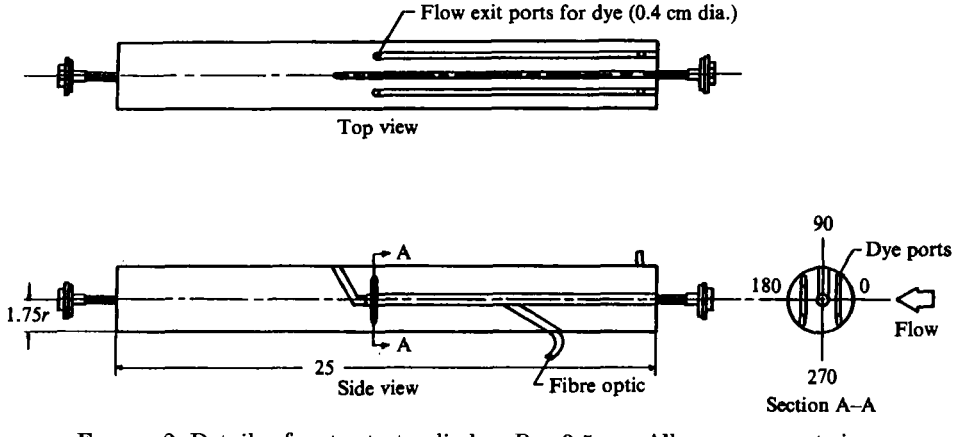

FIGURE 2. Details of water test cylinder, $D = 3.5$ cm. All measurements in cm.

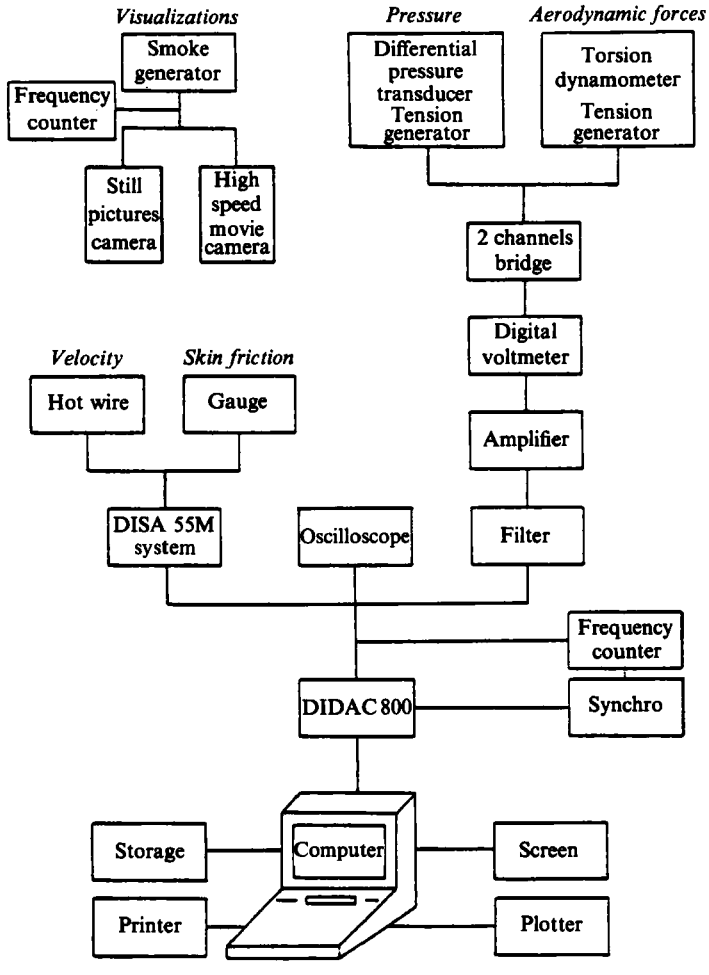

FIGURE 3. Block diagram of the IMFM wind-tunnel data acquisition system.

positioned 180° from the skin-friction gauge. The pressure signal was first amplified (Tranchant TX 200) and then filtered (Kronh–Hite 3341). Throughout the range of measurement, the output of the pressure probe was linear and the resonance frequency was well above the frequency range investigated. However, amplification and filtering are frequency dependent and therefore a calibrated signal was input to the data acquisition system at different frequencies. The amplitude and phase responses of the system were thus obtained as a function of the input frequency and included in the data treatment. Aerodynamic loads were directly measured with a torsion dynamometer described in detail by Valensi & Rebont (1972) (figure 4*b*). The output signal of the calibrated dynamometer was filtered and amplified.

Two Plexiglass cylinders of diameter 0.15 m and 0.20 m were tested in the wind tunnel. These cylinders, which spanned the entire test section, were mounted on the torsion dynamometer. Except during the measurement of forces, the top of the cylinder was attached to the upper wall. The overall system could be rotated with a position error of less than 0.5°. The angular position was changed for each skin-friction and pressure measurement. In order to shift from lift to drag, it was necessary to rotate the dynamometer by 90°. All probe signals were stored in a

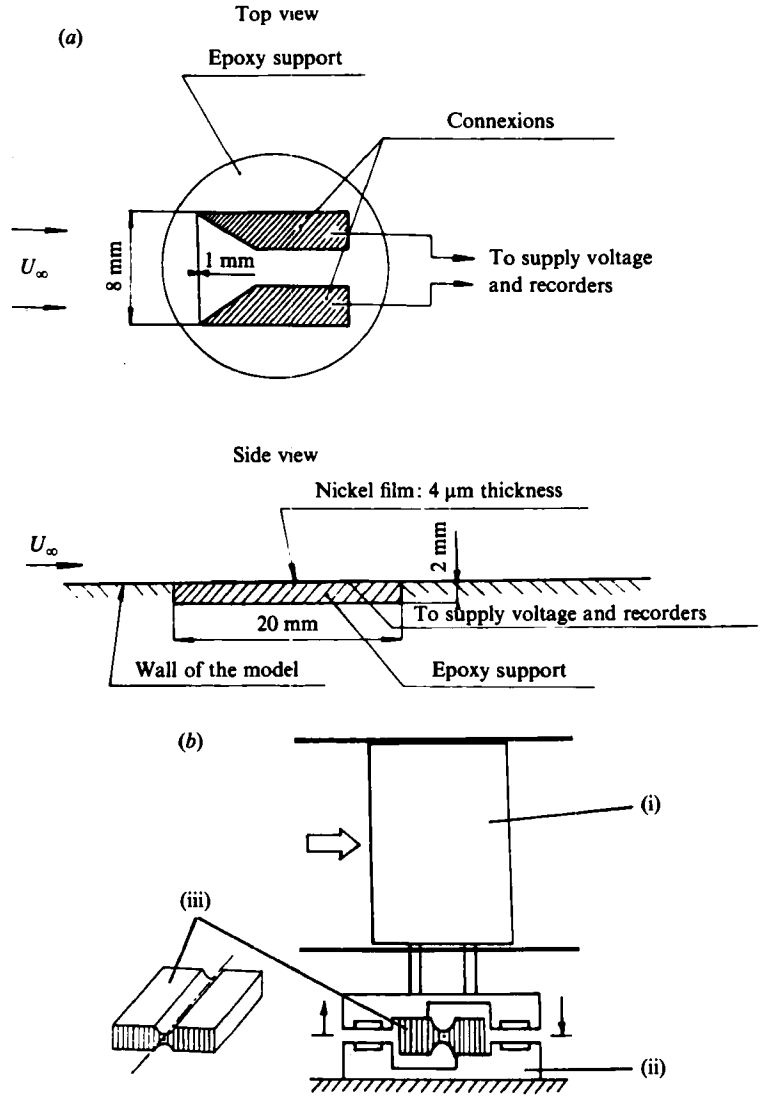

FIGURE 4. (a) Details of the skin-friction gauge. (b) Force measurement set-up: (i) cylinder; (ii) electromagnetic displacement sensor; (iii) calibrated torsion beam.

800-channel recorder (DIDAC 800), digitized and then reduced on a HP 9845 B minicomputer. In unsteady flow, a trigger signal was available and in this case 20 cycles could be recorded and averaged to improve the signal-to-noise ratio. Frequency-domain representations were obtained from a single time-domain record consisting of 512 data points over 19.7 s. This allowed a frequency precision of 0.05 Hz and a maximum frequency of 13 Hz using a discrete FFT routine stored in the HP computer. For presentation purposes, all frequency values were divided by the maximum value of the spectrum; thus the maximum plotted value is always unity.

Flow visualizations were obtained in both the water and the wind tunnels. In water, the flow was visualized by dyes emitted from the cylinder surface upstream and downstream of the point of separation. In air, smoke was used for still pictures and high-speed films (Fastax movie camera 300 frames/s).

3. Results

3.1. *Steady flow*

Preliminary experiments were conducted on circular cylinders in steady flow in air and in water. For Reynolds numbers from 45000 to 105000 in air and from 3200 to 110000 in water, the classical result of proportionality between the natural shedding frequency, F_{s0} and the Reynolds number has been verified via power spectra of velocity measurements at different points in the wake.

Typical data obtained on the cylinder under steady flow conditions are presented in figure 5 where we display pressure measurements for $D = 0.15$ and 0.20 m. A comparison is made with the results of Achenbach (1968) and Batham (1973). They compare well for $\theta < 50°$ (θ is defined in figure 5) and separation occurs, in each case, at around $\theta = 80°$. However, these values are consistently lower by about 15 %, after separation, when compared with those of Achenbach (1968) even though the tunnel blockage and the geometry were similar in both experiments. The differences in the free-stream turbulence levels and measurement techniques may be the reason of such data scattering, since a tunnel blockage of 20 % does not induce significant effects (Gonzalez 1980). It may be also noted that the Batham (1973) results are even lower after separation than our measurements.

The power spectra of the pressure signals at different angular positions indicate that at $\theta = 0°$, vortex shedding induces very small pressure fluctuations, as reported by McGregor (1957). Between $\theta = 30°$ and 150°, a sharp peak is present at the natural shedding frequency F_{s0} whereas at $\theta = 170°$ and 180° ($R_D = 3.3 \times 10^4$) a peak is observed at $2F_{s0}$. The two vortex arrays, shedding at F_{s0}, are symmetrical with respect to the probe position at $\theta = 180°$ and influence the probe as a single source shedding at $2F_{s0}$. Ferguson & Parkinson (1967) discuss a similar result.

In order to investigate the thin region next to the wall, the measurement of the skin friction is very useful even if, as in the present case, only qualitative results are obtained. For different angular positions, the output-voltage fluctuations of the skin-friction gauge $E = (E_0 - E_m)/E_m$ are plotted in figure 6, along five consecutive periods. E_m is the mean value of the signal E_0 recorded as a function of time. These records are characteristic of a laminar unsteady boundary layer. Five angular zones may be defined as follows:

(*a*) The first is a stagnation zone, whose angular extent, $-3 < \theta < +3°$, agrees with the results of Dwyer & McCroskey (1973). Because the skin-friction gauge is unable to sense the direction of the flow in the boundary layer, the signal is rectified and displays twice the shedding frequency. As shown in figure 6 ($\theta = 3°$), the limit of this zone is reached when the rectified part of the waveform disappears on the signal.

(*b*) The second zone is around 45°, where the amplitudes of the skin-friction variations are weaker. It is interesting to note that this position corresponds to a plateau on the skin-friction distribution (Achenbach 1968).

(*c*) Around $\theta = 70°$ the skin-friction fluctuations are larger. At this angular position there is a strong gradient of the mean skin friction (Achenbach 1968). For $R_D = 10^5$, results from Meier, Kreplin & Fang (1981) display the same behaviour. Thus, the amplitude variation of the skin friction at zone (*b*) and zone (*c*) is directly related to the mean skin-friction gradient.

(*d*) The fourth region is the zero-skin-friction zone whose limits are defined in the same way as for the stagnation point and are found at $75° \leqslant \theta \leqslant 90°$. Here again the frequency of oscillation is $2F_{s0}$.

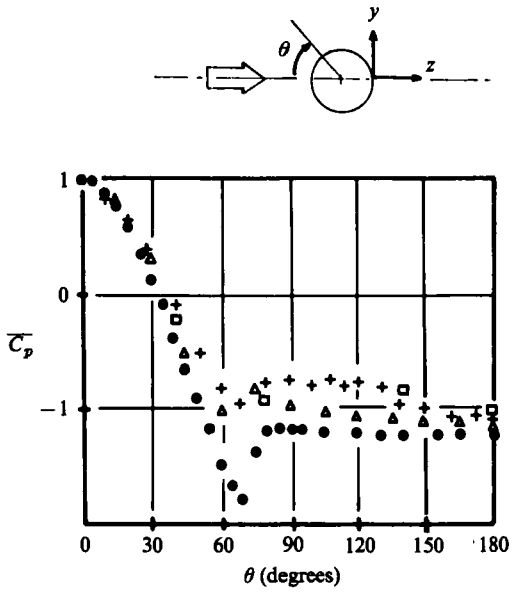

FIGURE 5. Pressure distribution around circular cylinder. ●, Achenbach (1968) $R_D = 10^5$; +, Batham (1973) $R_D = 1.1 \times 10^5$. Present study: △, $R_D = 3.3 \times 10^4$; □, $R_D = 9.3 \times 10^4$.

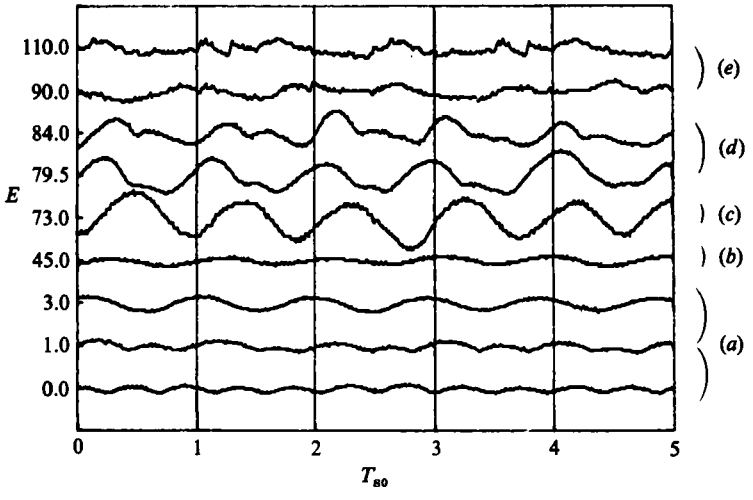

FIGURE 6. Instantaneous skin-friction signal, for $R_D = 46000$.

(*e*) Beyond $\theta = 90°$, the periodic trace is replaced by a higher frequency fluctuation, typical of a separated boundary layer.

The components of the aerodynamic force F_a have been measured for $R_D = 40000$. The lift coefficient is defined as $C_L = F_{ay}/(\frac{1}{2}\rho V_\infty^2 S)$, F_{ay} being the y-component of F_a. The coefficient C_L, presented in figure 7, oscillates between ± 0.7 at a frequency equal to F_{s0}: this value compares well with the results of So & Savkar (1981). The drag coefficient (figure 7), $C_D = F_{az}/(\frac{1}{2}\rho V_\infty^2 S)$ shows an amplitude of variation of ± 0.0375 around a mean value of 1.45. This mean value also agrees with that found by So & Savkar (1981). Their results as well as those of Ramamurthy & Ng (1973) confirm

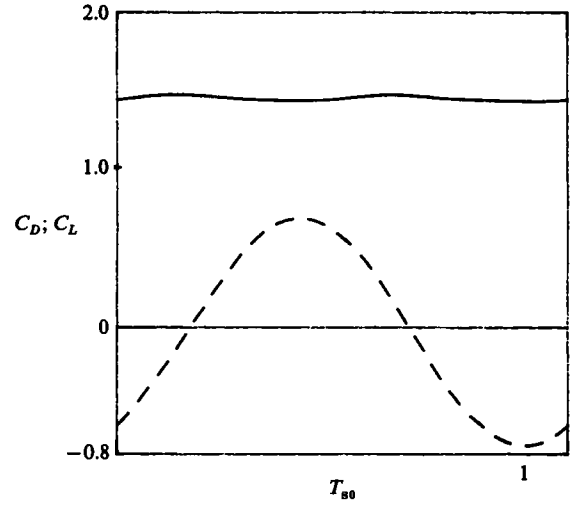

FIGURE 7. Instantaneous forces for $R_D = 40000$; ---, C_D; ——, C_L.

the small influence of a tunnel blockage of 20 % on the force measurements, as already discussed with regard to the pressure measurements.

However, our amplitude variation of C_D is smaller by a factor of almost one half compared with the So & Savkar results (1981). The ratio $\Delta C_L/\Delta C_D$ is equal to 18 whereas experimentally obtained values presented by King (1977) are around 10, again indicating the underestimation of ΔC_D by a factor of 2. Since ΔC_D is a very small quantity compared with the value of $C_D(\Delta C_D/2C_D = 2.6\,\%)$, its measure is of the same order of magnitude as the force measurement error. This ambiguity is not an important factor in the present study because the interest here is mainly in the frequency of the forces exerted on the cylinder.

3.2. *Oscillating flow*

The parameter A/D for forced motion of the cylinder corresponds to $\epsilon = \Delta V/\omega D$ for the case of a fixed cylinder in oscillatory flow, where ΔV is the amplitude of velocity variation and ω equals $2\pi F$, F being the imposed velocity frequency. In air, the parameter ϵ was kept at a value of 0.2 to ensure a sufficiently large threshold window for lock-on to occur. In water several values of ϵ were tested and an example for $\epsilon = 0.036$ is presented. The frequency F is increased step by step, each run being independent.

For different values of F, the power spectra of the velocity measurement in the wake are presented in figure 8. In this figure, the peaks at F are indicated with a circle and those at F_s with a star. The purpose of presenting such detailed data is to document the displacement of the two frequencies, F and F_s for small increments of F. In this figure, the behaviour of F_s before lock-on is unexpected. There is a progressive decrease of F_s as F increases, almost as if the driving frequency F slowly attracts the shedding frequency. They meet without even any particular changes in the power spectrum, after which F_s continues to decrease. This result is in good agreement with that of Tanida *et al.* (1973) for in-line oscillations of the cylinder, although the authors of that paper have not discussed this fact explicitly. The effect is not so pronounced in their results, because of the lower value of their amplitude ratio and it is possible that they have missed this important aspect of the flow.

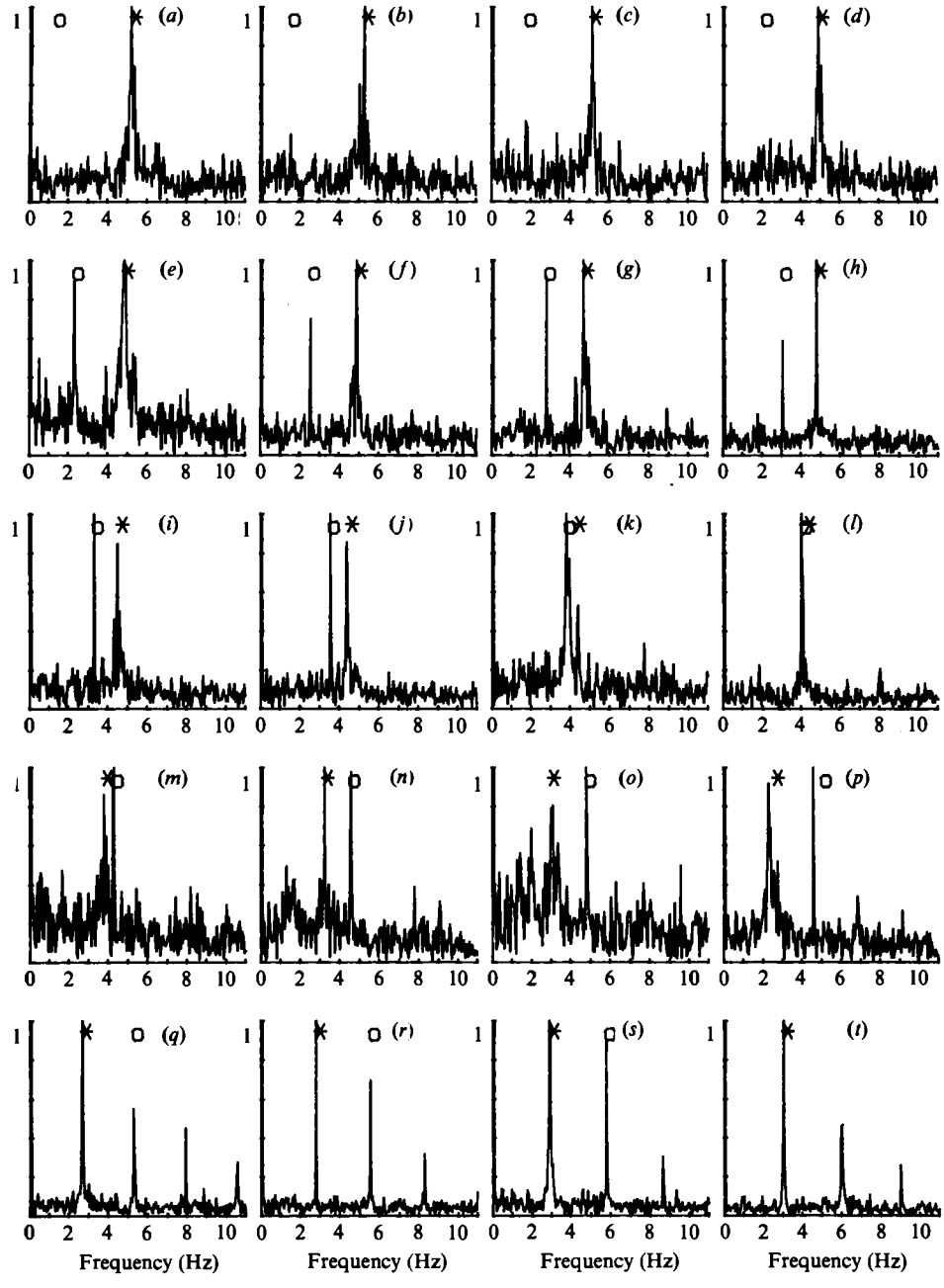

FIGURE 8. Power spectra of the velocity in the wake for $R_D = 35000$, $D = 0.15$ m, $F_{s0} = 5.38$ Hz, $\epsilon = 0.2$, $x = 0$, $y = 0.1$ m, $z = 0.4$ m (for coordinates x, y and z see figure 5); *, F_s; ○, F. (*a*) $F = 1.29$ Hz, $F_s = 5.14$ Hz; (*b*) 1.50 Hz, 5.19 Hz; (*c*) 1.75 Hz, 5.04 Hz; (*d*) 2.00 Hz, 4.82 Hz; (*e*) 2.25 Hz, 4.74 Hz; (*f*) 2.50 Hz, 4.82 Hz; (*g*) 2.75 Hz, 4.61 Hz; (*h*) 3.00 Hz, 4.72 Hz; (*i*) 3.25 Hz, 4.45 Hz; (*j*) 3.50 Hz, 4.35 Hz; (*k*) 3.75 Hz. 4.19 Hz; (*l*) 4.00 Hz, 4.13 Hz; (*m*) 4.26 Hz, 3.71 Hz; (*n*) 4.50 Hz, 3.13 Hz; (*o*) 4.76 Hz, 2.86 Hz; (*p*) 5.00 Hz, 2.49 Hz; (*q*) 5.26 Hz, 2.60 Hz; (*r*) 5.49 Hz, 2.73 Hz; (*s*) 5.75 Hz, 2.86 Hz; (*t*) 5.99 Hz, 2.97 Hz.

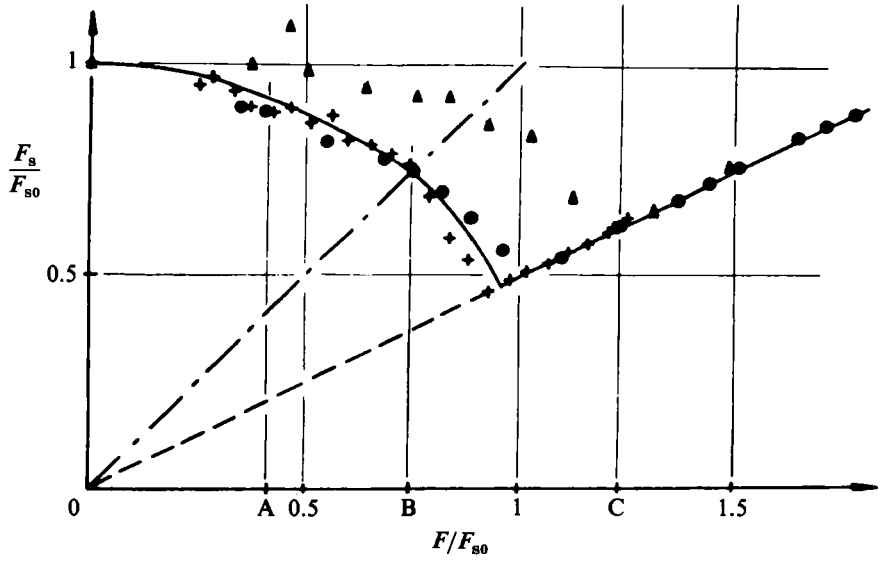

FIGURE 9. Variation of F_s/F_{s0} with F/F_{s0}: ▲, $A/D = 0.14$ Tanida *et al.* (1973). Present study: ●, $\epsilon = 0.2$, $D = 0.15$ m, $R_D = 35000$; +, $\epsilon = 0.2$, $D = 0.20$ m, $R_D = 40000$. —·—, $F_s/F_{s0} = F/F_{s0}$; — — —, $F_s/F_{s0} = \frac{1}{2}F/F_{s0}$; ——, mean fitting curve.

Occurrence of the lock-on appears clearly. It starts at around $F/F_{s0} = 1$ with a synchronization of F and F_s, but then the ratio F_s/F is 0.5 as expected from results for in-line vibrating cylinders (Griffin & Ramberg 1976). The shedding frequency is then equal to the subharmonic of the driving frequency. During lock-on, the flow in the wake is quite organized as mentioned by Ferguson & Parkinson (1967) and by Bishop & Hassan (1964); both frequency-domain and time-domain plots are typical of this trend. The wake flow is organized around large structures having specific frequencies.

These results for $D = 0.15$ and 0.20 m in addition to those of Tanida *et al.* (1973) are superimposed in a composite plot displayed in figure 9. The fact that two curves are not coincident during the capture phase is due only to different amplitude parameters ($A/D = 0.14$ and $\epsilon = 0.20$).

In figure 10 data obtained in water are presented for $\epsilon = 0.036$ and $R_D = 3000$. Because of the lower value of the parameter ϵ, clear lock-on characteristics are evident when the driving frequency is around twice the natural shedding frequency. Again, the shedding frequency is locked to the subharmonic of the driving frequency. Before lock-on, the frequency of shedding decreases slightly. Lock-on ends with a smooth transition before the vortices are shed at the natural Strouhal frequency. At the highest range of the scale there is some evidence of the lock-on around $F/F_{s0} = 4$, but there is insufficient data to draw any relevant conclusions.

The lock-on limits obtained during this study have been added to those previously recorded by Griffin & Ramberg (1976) for the case of in-line oscillating cylinders (figure 11). One of the present results, for $2\epsilon = 0.4$, does not exactly fit the trend of the other data, but the results of Tanida *et al.* (1973) indicate an increase of the bounds of the lock-on with the Reynolds number. The Reynolds-number effect could explain this discrepancy. It should be noted however, that results presented by Stansby (1976) for transverse oscillation show an opposite influence of the Reynolds number.

A detailed investigation has been performed for three values of F, (points A, B, C on

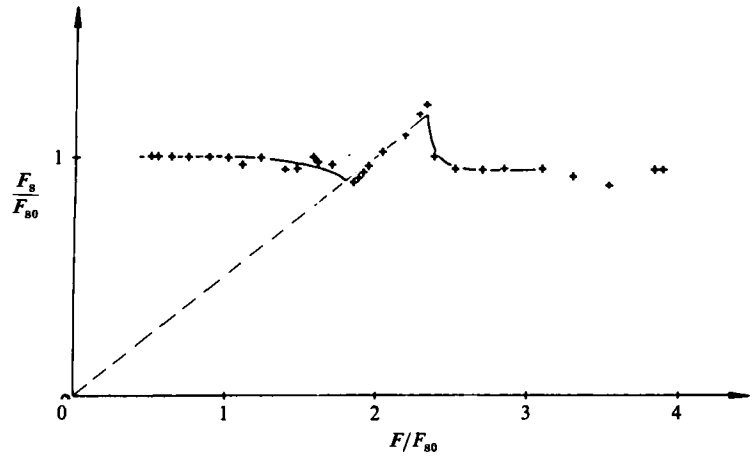

FIGURE 10. Variation of F_s/F_{s0} with F/F_{s0}: +, $\epsilon = 0.36$, $D = 0.035$ m, $R_D = 3000$.

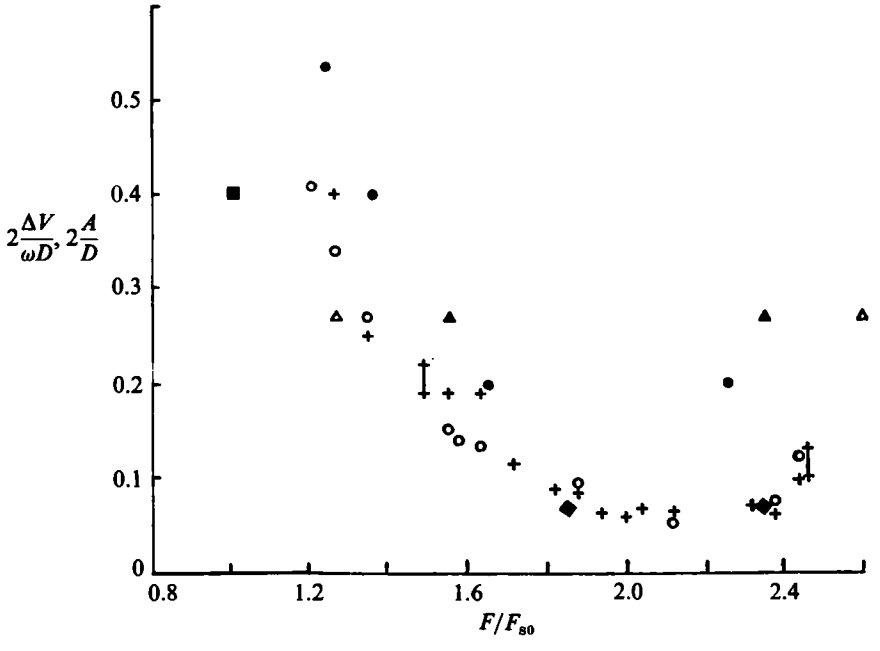

FIGURE 11. Limits of the locking-on as a function of the amplitude and frequency for in-line oscillation: +, ○, $R_D = 190$, Griffin & Ramberg (1976); ▲, $R_D = 80$; △, $R_D = 4000$, Tanida *et al.* (1973); ●, $R_D = 100$, Tatsuno (1972); and for flow oscillation present study: ◪, $R_D = 3000$; ■, $R_D = 40000$.

the abscissa of figure 9). Typical values related to these points are summarized in table 1. Lift and drag measurements are presented in both time and frequency domains for cases A, B and C in figure 12 and they are compared with velocity spectra in the wake. The lift follows the vortex-shedding rhythm, regardless of the imposed flow pulsation frequency. The driving-frequency peak, visible in the velocity spectra does not appear in those for the lift. Before lock-on, ΔC_L decreases from 1.2 to 0.45 as soon as F/F_s equals 0.41 (case A), but increases to 2.23 during lock-on.

In steady conditions, the drag frequency is twice the shedding frequency. In

	A	B	C
F/F_{s0}	0.41	0.71	1.23
F_s/F_{s0}	0.82	0.71	0.62
F_s/F	2	1	0.5
	not locked	locked	

TABLE 1. Shedding frequencies and driving frequencies for cases A, B and C

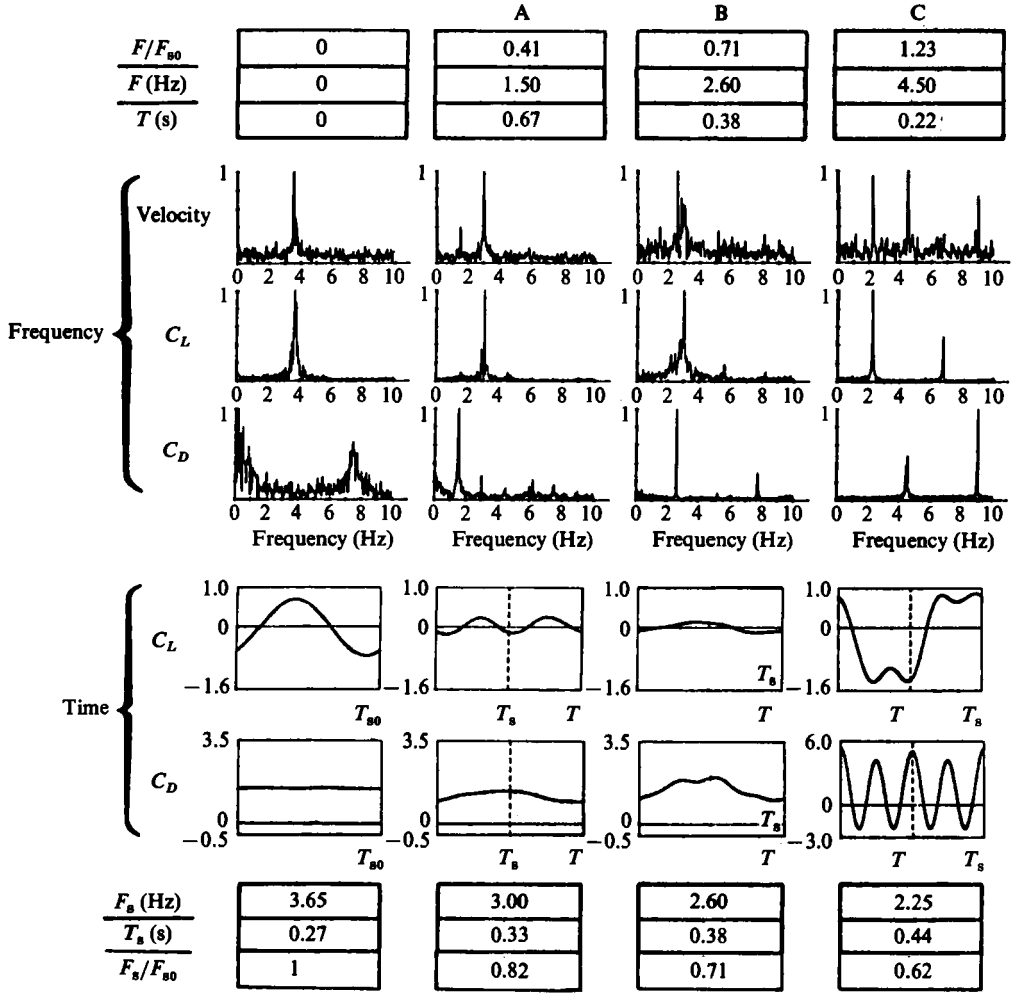

FIGURE 12. (*a*) Frequency and (*b*) time representation of lift and drag coefficients compared to velocity spectra for steady and unsteady flow: $R_D = 40000$, $D = 0.20$ m.

unsteady flow, owing to the velocity variation, an in-line aerodynamic component proportional to λ^2 should be added to F_s. Since the drag fluctuation is weak for steady flow, the effect of the flow oscillation is predominant on the drag and thus it varies with a frequency equal to F. A small peak at $2F_s$ still remains in case A, which corresponds to the smallest value of λ.

Keeping ϵ constant as F increases, implies an increase of ΔV and thus of

λ ($\lambda = 0.125$ for case A, 0.216 for case B and 0.352 for case C). This induces in turn an increase in ΔC_D. The experimental value obtained here is $\Delta C_D = 7$. The ratio $\Delta C_L/\Delta C_D$ is less than unity for all values of F, which is a sharp decrease from steady values.

The pressure fluctuations are measured at different angular positions for driving frequencies corresponding to cases A, B and C. The mean values of C_p are close to steady values. The increase in λ induces larger variations of C_p as already noted for the force measurements (cases A–C). The frequency of the pressure fluctuations follows that of the unsteady flow velocity.

Skin-friction measurements for cases A, B and C confirm the angular division of the cylinder into five zones. It is well confirmed from the spectrum analysis of the skin-friction signal that the shedding process drives the skin-friction variations and thus the boundary-layer fluctuations with the shedding frequency. However, the outer flow pulsation also influences the skin-friction response and a peak of lower magnitude, at the driving frequency, is present on most of the spectra.

The stagnation zone increases from $\pm 3°$ (case A) to $\pm 7.5°$ (case C). As in steady flow, at around $\theta = 45°$ the amplitude of the fluctuation is reduced, whereas near $\theta = 70°$ it is amplified. Near $\theta = 45°$, the profiles for cases A and C show a superimposed fluctuation at the driving frequency, a phenomenon well confirmed by spectrum analysis. Transition may be suspected for case C at $\theta = 66°$ because high frequencies are added to the periodic trace, although they seem to be no longer present on the following waveforms.

The separation zone is amplified from $\theta = 76°$–$89°$ (case A) up to 75°–97° (case C) but on some records it reaches $\theta = 110°$ during a few periods (cases B, C). For transverse oscillations, Mei & Currie (1969) found that the amplitude of the separation zone increases up to $F/F_{s0} = 0.9$. The regular increase of the displacement of the separation point with F/F_{s0} in the present study indicates a similar behaviour. In the case of flow oscillations, the maximum amplitude should be found at around $F/F_{s0} = 2$; however this cannot be reached with the present oscillating mechanism of the wind tunnel.

Flow visualization of the wake of oscillating cylinders reveals different flow patterns than the usual alternate Kármán vortex street. Griffin & Ramberg (1976) distinguish two fundamental vortex patterns in their experiments: depending on the driving frequency, one or two vortices were shed during each cycle. The present visualizations in air are shown in figure 13 and in water in figure 14. When F/F_{s0} is small (figures 13*a*, 14*a*) the vortex-street geometry is similar to that corresponding to steady conditions, in agreement with all previous measurements. For $F/F_{s0} = 1$ (figures 13*b*, 14*b*) two symmetric vortices are shed simultaneously during one cycle. This pattern has been observed to be more stable in water than in air. This is probably due more to a different Reynolds number for each experiment than to the difference in the cylinder aspect ratio (0.3 and 0.4 in air and 0.12 in water). The difference in the aspect ratio has no significant influence on the previous results, especially on the progressive frequency attraction before lock-on. This surprising arrangement of the wake has also been noted for in-line oscillations of the cylinder (King 1977).

In the lock-on range (figures 13*c*, 14*c*), the influence of the flow oscillation is very strong. During one period of the flow oscillation, the vortex remains close to the cylinder as it forms and grows, even closer in fact than before locking-on. It absorbs the counter-rotating vortex that would normally develop and then sheds it, creating a sudden rolling of the wake towards the opposite side. A new vortex of the opposite

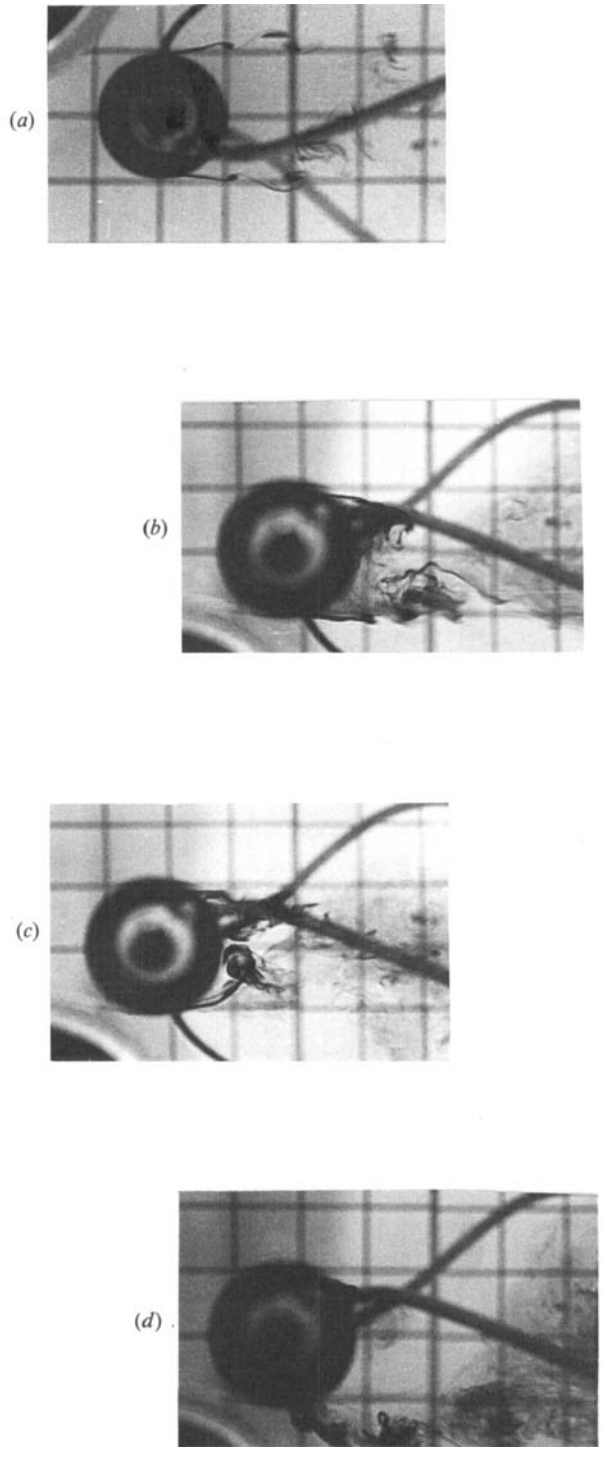

FIGURE 13. Flow visualization of the wake in water: $D = 0.035$ m, $R_D = 3000$, $F_{s0} = 0.53$ Hz. (*a*) steady flow; (*b*) $F = 0.43$ Hz; (*c*) $F = 0.53$ Hz; (*d*) $F = 0.63$ Hz.

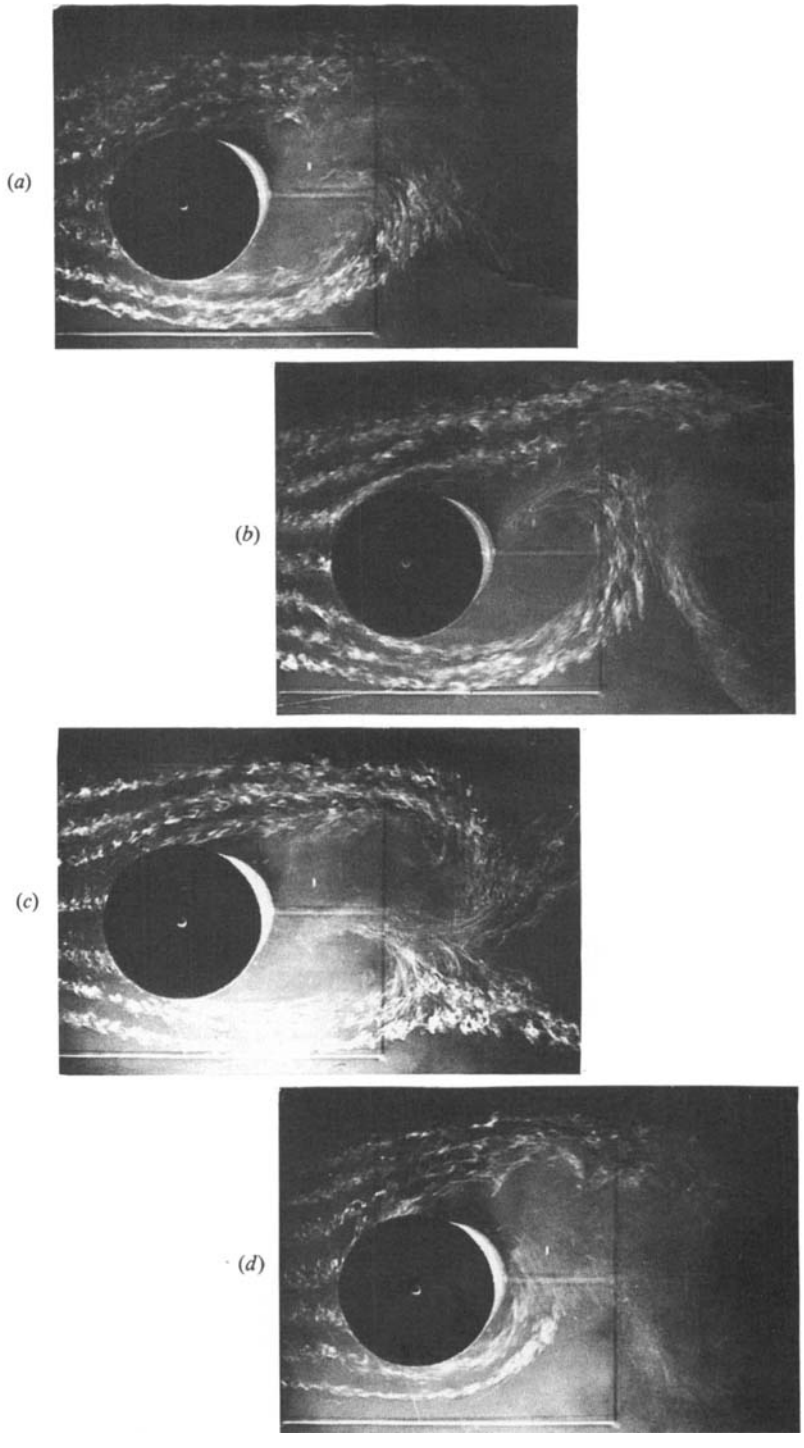

FIGURE 14. Flow visualization of the wake in air: $D = 0.2$ m, $R_D = 40000$, $F_{s0} = 3.65$ Hz. (*a*) steady flow; (*b*) $F = 1.5$ Hz; (*c*) $F = 2.6$ Hz; (*d*) $F = 4.5$ Hz.

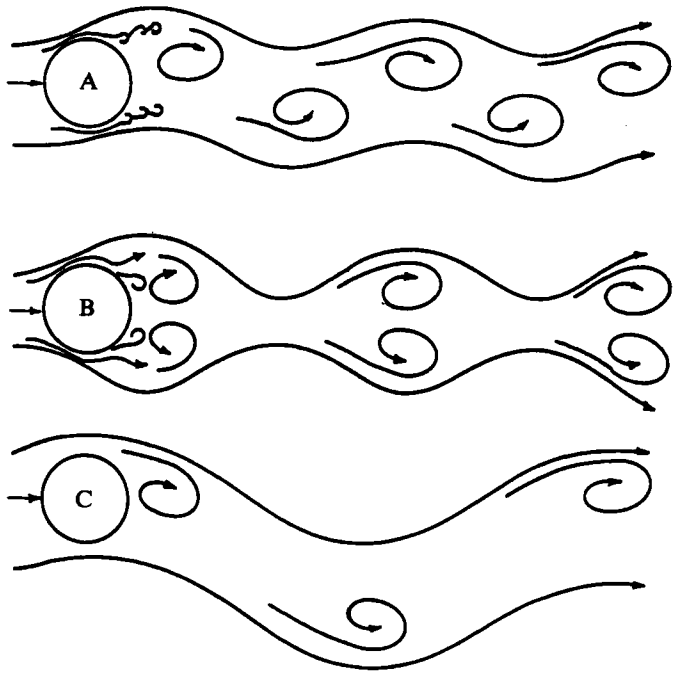

FIGURE 15. Schematic representation of vortex-shedding patterns. Cases A, B and C correspond to the conditions of table 1.

sign develops during the next period. This is the physical representation of the relationship, already pointed out, between F_s and F during lock-on ($F_s = 0.5F$): one vortex is shed during a period of oscillation of the flow. The visualizations also reveal the large amplitude of the stagnation and separation zones. A sketch of these three flow patterns, which also appear in Jones (1980) and Jones *et al.* (1981 *a*), is presented in figure 15.

4. Conclusions

The following conclusions can be drawn from the results of this study.

(i) The occurrence of lock-on is demonstrated, which indicates that the amplitude ratio ϵ and the frequency range were too low in Hatfield & Morkovin experiments (1973).

(ii) The results in air are similar to those in water. Both measurements confirm the progressive attraction of the shedding frequency F_s before lock-on. This is very significant; until now, it was believed that the shedding frequency would equal either the natural frequency or the driving frequency for transverse oscillations or half of this value for in-line oscillations. Our experiments indicate that the shedding frequency may drift towards the driving frequency.

(iii) The general features of locking-on observed for in-line oscillations have been confirmed in oscillating flow:

$F_s/F = 0.5$;

lock-on is found around $F = 2F_{s0}$, and there is some evidence that lock-on may occur at $F = 4F_{s0}$ as well;

a wake organized around large structures of narrowband energy revealed by

clear peaks in the spectra and regular time-domain measurements. These trends were present for all measured quantities;

two different flow patterns: symmetric vortex shedding at $F/F_s = 1$ and alternate vortex shedding during lock-on.

(iv) A sharp decrease of the lift-to-drag fluctuation ratio is observed in unsteady conditions, even for low values of F.

The work at VPI & SU was supported by the Department of Energy, Grant no. DE-A505-82ER12022. This was part of the programme of Dr Oscar P. Manley, Division of Engineering, Mathematics and Geosciences of the Office of Basic Energy Sciences.

REFERENCES

ACHENBACH, E. 1968 *J. Fluid Mech.* **34**, 625.

BARBI, C., FAVIER, D. & MARESCA, C. 1981 In *Proc. IUTAM Symp. Turbulent Shear Flow*, p. 248. Springer.

BATHAM, J. P. 1973 *J. Fluid Mech.* **57**, 209.

BISHOP, R. E. & HASSAN, A. Y. 1964 *Proc. R. Soc. Lond.* A **227**, 51.

CHEN, Y. N. 1968 *J. Engng. Ind.* **90**, 134.

DWYER, H. A. & MCCROSKEY, W. J. 1973 *J. Fluid Mech.* **61**, 753.

ERICSSON, L. E. 1980 *AIAA J.* **18**, 935

FERGUSON, N. & PARKINSON, G. V. 1967 *J. Engng Ind.* **89**, 831.

GONZALEZ, M. 1980 Thèse de Doctorat Ingénieur, Lyon, France (in French). Contribution à l'étude de l'aerodynamisme d'un prisme à section carrée placé en écoulement confiné.

GRIFFIN, O. M. & RAMBERG, S. E. 1976 *J. Fluid Mech.* **75**, 257.

HATFIELD, H. M. & MORKOVIN, M. V. 1973 *Trans. ASME* I: *J. Fluid Engng* **95**, 249.

JONES, G. S. 1980 M.Sc. thesis, Virginia Polytechnic Institute and State University, Va. USA. Measurement and visualization of vortex shedding natural and forced.

JONES, G. S., BARBI, C. & TELIONIS, D. P. 1981*a* In *Proc. IUTAM Symp. Turbulent Shear Flow*, p. 228. Springer.

JONES, G. S., TELIONIS, D. P. & BARBI, C. 1981*b* *AIAA paper* 81-0053.

KING, R. 1977 *Ocean Engng* **4**, 141.

KOROMILAS, C. A. & TELIONIS, D. P. 1980 *J. Fluid Mech.* **97**, 347.

MCGREGOR, D. M. 1957 *University of Toronto Institute for Aerospace Studies, Tech. Note* 14.

MARESCA, C., FAVIER, D. & REBONT, J. 1978 In *15e Colloque d'aérodynamique appliquée, Marseille, France* (in French).

MARESCA, C., REBONT, J. & VALENSI, J. 1975 In *Symp. on Unsteady Aerodynamics* (ed. R. B. Kinney), vol. 1, p. 35.

MEI, V. C. & CURRIE, I. G. 1969 *Phys. Fluids*, **12**, 2248.

MEIER, H. U., KREPLIN, H. P. & FANG, L. W. 1981 In *Proc. IUTAM Symp. Turbulent Shear Flow*, p. 87. Springer.

RAMAMURTHY, A. S. & NG, C. P. 1973 *Proc. Inst. Civil Engrs* **49**, 269.

SAGNER, M. 1981 In *18e Colloque d'aérodynamique appliquée, Poitiers, France* (in French).

SAINSBURY, R. N. & KING, D. 1971 *Proc. Inst. Civ. Engrs* **49**, 269.

SO, R. M. C. & SAVKAR, S. D. 1981 *J. Fluid Mech.* **105**, 397.

STANSBY, P. K. 1976 *J. Fluid Mech.* **74**, 641.

TANIDA, Y., OKAJIMA, A. & WATANABE, Y. 1973 *J. Fluid Mech.* **61**, 769.

TATSUNO, M. 1972 *Bull. Res. Inst. Appl. Mech., Kyushu University*, **36**, 25.

VALENSI, J. & REBONT, J. 1972 In *Proc. AGARD FDP Meeting Aerodynamics of Rotary Wings, Marseille, France*, CPP III, 12 (in French).